Hydrazine Cation Radical in the Active Site of Ethanolamine Ammonia-Lyase: Mechanism-Based Inactivation by Hydroxyethylhydrazine†

Vahe Bandarian‡ and George H. Reed*

Institute for Enzyme Research, Graduate School, and Department of Biochemistry, College of Agricultural and Life Sciences, University of Wisconsin−Madison, 1710 University Avenue, Madison, Wisconsin 53705

Received March 18, 1999; Revised Manuscript Received June 28, 1999

ABSTRACT: A study has been made of the mechanism of inactivation of the adenosylcobalamin-dependent enzyme, ethanolamine ammonia-lyase (EAL), by hydroxyethylhydrazine. Incubation of EAL with adenosylcobalamin and hydroxyethylhydrazine, an analogue of ethanolamine, leads to rapid and complete loss of enzymic activity. Equimolar quantities of 5′-deoxyadenosine, cob(II)alamin (B_{12r}), hydrazine cation radical, and acetaldehyde are products of the inactivation. Inactivation is attributed to the tight binding of B_{12r} in the active site. Removal of B_{12r} from the protein by ammonium sulfate precipitation under acidic conditions, however, restores significant activity. This inactivation event has also been monitored by electron paramagnetic resonance (EPR) spectroscopy. In addition to EPR signals associated with B_{12r}, spectra of samples of inactivation mixtures reveal the presence of another radical. The other radical is bound in the active site where it undergoes weak magnetic interactions with the low spin Co^{2+} in B_{12r}. The radical species was unambiguously identified as a hydrazine cation radical by using [$^{15}N_2$]hydroxyethylhydrazine, ^2H_2O, and quantitative interpretation of the EPR spectra. Homolytic fragmentation of a hydroxyethylhydrazine radical to acetaldehyde and a hydrazine cation radical is consistent with all of the observations. All of the experiments indicate that the mechanism-based inactivation of EAL by hydroxyethylhydrazine results from irreversible cleavage of the cofactor and tight binding of B_{12r} to the active site.

The coenzyme B_{12}[1] dependent enzyme, ethanolamine ammonia-lyase (EAL; EC 4.3.1.7), catalyzes the conversion of ethanolamine to ammonia and acetaldehyde (*1*−*3*). Bacteria which possess the genes for EAL can grow on ethanolamine as the sole source of carbon and nitrogen (*1, 4*). Evidence indicates that the reaction catalyzed by EAL proceeds by a radical mechanism wherein a cofactor-derived 5′-deoxyadenosyl radical (directly or indirectly) abstracts a hydrogen atom from C-1 of the substrate to generate a substrate-based radical. The substrate radical rearranges to the product radical which acquires a hydrogen atom from 5′-deoxyadenosine to give product. Reformation of the cobalt carbon bond restores the cofactor and completes the catalytic cycle (*2, 3*).

The radical reaction mechanism of EAL makes the enzyme susceptible to inactivation by analogues of the substrate that allow the radical intermediates to stray from the main catalytic pathway (*5, 6*). B_{12r}—a product of the homolytic cleavage of coenzyme B_{12}—binds with high affinity to EAL and can only be removed by harsh treatments (*7*). Hence, aberrant reaction pathways that abandon B_{12r} in the active site incapacitate further catalysis. Rogue radical intermediates could also exact irreversible damage to the enzyme or the cofactor fragments (*8*). An analysis of the products of these inactivation reactions can provide information about the sequence of radical transformations leading up to inactivation (*9*−*12*). Quantitative analysis of the products of inactivation can also provide information on the number of active sites present in the enzyme. For EAL, estimates of the number of active sites vary between 2 and 6 for the $\alpha_6\beta_6$ oligomer (*13*−*16*).

Screening of various substituted, short-chain alcohols for reaction with EAL revealed hydroxyethylhydrazine (HEH) to be an exceptionally efficient inactivator of the enzyme. EPR spectra of reaction mixtures revealed unusual signals for B_{12r} and a robust signal for another radical. Analysis of the products of the reaction and of the EPR spectra provide a clear indication of the pathway for inactivation and geometrical information on the position of radicals within the active site. The present paper reports the results of these experiments.

EXPERIMENTAL PROCEDURES

Materials. Yeast alcohol dehydrogenase, NADH, coenzyme B_{12}, and 5′-deoxyadenosine were purchased from Sigma. Hepes was from Research Organics and Tris was from Fisher. Lysozyme (from hen egg white) and DNase I (from bovine pancreas) were from Boehringer-Mannheim. Unlabeled hydroxyethylhydrazine was from Lancaster. 2,4-

† This research was supported by NIH Grant GM35752.

* To whom correspondence should be addressed. Phone: (608) 262-0509. Fax: (608) 265-2904.

‡ Present address: Univ. Michigan, Biophys. Res. Div., Chem. Sci. Bldg., 930 N University, Ann Arbor, MI 48109-1055.

[1] Abbreviations: B_{12r}, cob(II)alamin; coenzyme B_{12}, adenosylcobalamin; EPR, electron paramagnetic resonance; EAL, ethanolamine ammonia-lyase; HEH, hydroxyethylhydrazine; Hepes, *N*-2-hydroxyethylpiperazine-*N*′-2-ethane-sulfonic acid; HPLC, high-pressure liquid chromatography; hydroxo-B_{12}, hydroxocobalamin; IU, international unit; TLC, thin-layer chromatography; Tris, tris (hydroxymethyl)aminomethane; SDS−PAGE, sodium dodecyl sulfate−polyacrylamide gel electrophoresis; zfs, zero-field splitting.

10.1021/bi990620g CCC: $18.00
Published on Web 08/31/1999

Dinitrophenylhydrazine, ethanolamine, and ^2H_2O were purchased from Aldrich. 2,4-Dinitrophenylhydrazine was recrystallized from ethyl acetate prior to use. [^{15}N]Hydrazine (99% ^{15}N) was purchased from Isotec, and [1,1,2,2-$^2H_4$]-bromoethanol (98% ^{2}H) was from Cambridge Isotope Labs. Competent BL21(DE3)pLysS cells were purchased from Novagen.

Subcloning and Expression of EAL. The plasmid pKQE4.5 (*17*) encoding the large and small subunits of the *Salmonella typhimurium* EAL was a generous gift from Dr. Bernard Babior. The pTZE vector (*18*) was kindly provided by Dr. Barbara Swanson. The pKQE4.5 vector was digested by Bsu36I and purified, and the digested site was filled-in using the Klenow polymerase fragment. The resulting singly cut vector was purified and digested with *Hin*dIII. This digest released a DNA fragment that contained both the large and small subunits of EAL. The pTZE vector was digested with *Xcm*I and *Hin*dIII and ligated to the genes for EAL. The resulting vector, pTEAL, was used for all subsequent expression experiments. Competent BL21(DE3)pLysS cells were transformed with pTEAL and plated onto LB plates containing 100 μg mL^{-1} ampicillin and incubated at 37 °C overnight. A single colony was picked from this plate and transferred to a 0.5 L starter culture (with 0.1 mg mL^{-1} ampicillin). The starter was shaken at 37 °C until turbid (OD $\approx$ 0.1−0.3) and aliquots were used to initiate large scale growth (typically 12 2 L flasks containing 1 L of LB and 0.1 mg mL^{-1} ampicillin in each). The cultures grew overnight at 37 °C. Cells were harvested by centrifugation at 4000*g*, and the cell pastes frozen in liquid N_2. Cell yields per liter of culture were 3−4 g.

Enzyme Purification. The enzyme purification is based on the limited solubility of EAL near neutral pH in buffers that also contain glycerol. All steps were carried out at 4 °C. Cell pastes (40−50 g) were thawed in 0.20 L of 50 mM Hepes/NaOH, pH 7.5, also containing 10% glycerol, 50 mg of lysozyme, 1 mg of DNase, and 1 mM phenylmethanesulfonylflouride. The suspension was stirred for 1 h and then centrifuged at 17000*g* for 30 min. The supernatant was discarded, and the pellet was suspended in 0.4−0.5 L of 50 mM Hepes/NaOH, pH 7.5. The mixture was centrifuged at 17000*g* for 30 min, and the supernatant brought to 15% saturation with solid ammonium sulfate over 20 min. The suspension was stirred 20−30 min and centrifuged at 17000*g* for 30 min. EAL, precipitated by ammonium sulfate under these conditions, forms a translucent pellet or film. The precipitate was suspended in ~150 mL of 10 mM Hepes/NaOH, pH 7.5. The suspension was dialyzed versus 2 × 2 L of 10 mM Hepes/NaOH, pH 7.5 overnight. During the course of the dialysis, the suspension clears, forming a nearly homogeneous solution of EAL. At this stage, the protein concentration is typically ~2−3 mg mL^{-1}. The contents of the dialysis bag were centrifuged at 17000*g* for 30 min and the supernatant concentrated in Amicon concentrator (YM30 membrane). This protocol typically yields 300−450 mg of EAL with specific activity of ~45−55 IU mg^{-1}. EAL purified by this protocol is >90% pure as judged by SDS−PAGE. The concentrated enzyme was stored at −80 °C. EAL used in these studies had a specific activity of ~52 IU mg^{-1}. Specific activities of EAL from *Clostridium sp.* have been in the range 15−45 IU mg^{-1} (*19, 20*), whereas for the recombinant enzyme from *S. typhimurium*, the published purification yielded enzyme with a specific activity of 25 IU mg^{-1} (*15*). The extinction coefficient calculated for $\alpha_6\beta_6$ oligomer using the program PEPTIDESORT (Genetics Computer Group, Madison) is 0.69 mL mg^{-1} cm^{-1}.

Inactivation Kinetics. EAL was incubated with HEH and coenzyme B_{12}, and at various times, aliquots were withdrawn and assayed for activity. The incubations were prepared by mixing EAL (5 μL of 26 mg mL^{-1}), coenzyme B_{12} (0.17 mM), 19 mM Hepes/NaOH, pH 7.5, and HEH (10 mM) in a total volume of 20 μL. Aliquots (5 μL) were withdrawn, diluted to 0.50 mL with 10 mM Hepes/NaOH, pH 7.5, and assayed for activity. The assay mixtures contained Hepes/NaOH, pH 7.5 (50 mM), ethanolamine (10 mM), yeast alcohol dehydrogenase (45 IU), NADH (0.13 mM), and coenzyme B_{12} (17 μM) in a total volume of 1 mL. Assays were initiated by adding 5 μL of the diluted (1:100) preincubation mixture.

Inactivation/Reactivation. EAL (200 μL of ~26 mg mL^{-1}) was mixed with coenzyme B_{12} (0.34 mM), HEH (10 mM), and Hepes/NaOH, pH 7.5 (15 mM), in a total volume of 0.40 mL. Samples were withdrawn, diluted, and assayed as described in the previous section. After a 30 min incubation, the reaction mixture was placed in dialysis against 1 L of 10 mM Hepes/NaOH, pH 7.5; the buffer was changed once. The inactivated EAL was removed from dialysis and assayed for activity with ethanolamine. In a separate experiment, EAL, which had been inactivated by HEH and dialyzed as described above, was resolved of bound cofactor by precipitation with ammonium sulfate under acidic conditions (*7*). The ammonium sulfate pellet was resuspended in ~2−3 mL of 10 mM Hepes/NaOH, pH 7.5, and dialyzed against 2 × 1 L of the same buffer. The protein was removed from dialysis and assayed for activity with ethanolamine as substrate. Protein concentration was determined by A_{280nm} measurements.

UV−Vis Profile of the Inactivation. To determine the UV−vis profile of EAL during the inactivation and to determine the stoichiometry of B_{12r} to EAL, absorption spectra were obtained before and after mixing EAL with coenzyme B_{12} and HEH. For these experiments, EAL (100 μL of ~26 mg mL^{-1}) and Hepes/NaOH, pH 7.5 (20 mM), were placed in one side of a split cuvette and diluted to a total volume of 0.8 mL. A mixture of HEH (10 mM), Hepes/NaOH, pH 7.5 (20 mM), and coenzyme B_{12} (85 μM) in a total volume of 0.8 mL was placed in the other compartment. Absorption spectra were obtained prior to and at various times after mixing the contents of the two chambers. The stoichiometry of B_{12r} to EAL was determined by following the loss of the 525 nm peak of coenzyme B_{12} using the difference extinction coefficient of B_{12r} ($\Delta\epsilon_{525nm} \approx 4.0$ mM^{-1} cm^{-1}) (*16, 21*).

Detection and Quantitation of 5′-Deoxyadenosine. Assay mixtures contained coenzyme B_{12} (0.17 mM), HEH (10 mM), Hepes/NaOH, pH 7.5 (16 mM), and EAL (25 μL of 26 mg mL^{-1}) in a total of 0.1 mL. The reactions were initiated by the addition of EAL and allowed to proceed for 15 min. The reactions were quenched by adding 0.1 mL of 1 N HCl, and the precipitated protein was removed by centrifugation. The supernatant was neutralized with 0.1 mL of 1 M Tris base. Aliquots of the neutralized reaction mixtures were analyzed by HPLC over a reversed-phase C-18 column (Rainin) using a gradient from 0 to 100% methanol in water. The peak areas

were compared with those obtained with 5′-deoxyadenosine solutions of known concentrations. The identity of the eluant was further confirmed by co-injection of the reaction mixture with authentic samples of 5′-deoxyadenosine.

Detection and Quantitation of Acetaldehyde. Acetaldehyde was converted to its 2,4-dinitrophenylhydrazone adduct and detected by HPLC. The reactions were setup as described above for the experiments in which 5′-deoxyadenosine was measured. The mixtures were quenched with 10 μL of 20 mM 2,4-dinitrophenylhydrazine in 3 N sulfuric acid. Precipitated protein was removed by centrifugation. Aliquots of the supernatant (40 μL) were neutralized with 1 M Tris base (25 μL) before injection onto a C-18 reversed-phase HPLC column. The hydrazone derivative was eluted isocratically with acetonitrile/water (60:40) and detected at 350 nm. The retention time for the hydrazone was ~6.9 min. Peak heights in the chromatogram were compared to those of solutions of authentic adduct ($\epsilon \approx 19$ mM^{-1} cm^{-1} in methanol) (*22*).

Synthesis of [1,1,2,2-$^2H_4$]Hydroxyethylhydrazine Hydrochloride. To a solution of 9 mmol of KOH in ethanol was added 14 mmol of hydrazine. [1,1,2,2-$^2H_4$]Bromoethanol (7 mmol) was added dropwise over 10 min, and the reaction was allowed to proceed 3 h. The reaction mixture was filtered, diluted to 0.5 L with water, and chromatographed on Dowex 50 × 8 (H^+ form). The resin was washed with water, and HEH was eluted with 1 N HCl. The eluate was neutralized and reduced to dryness by rotary evaporation. The resulting solid was then resuspended in ethanol and filtered and the filtrate reduced to dryness to obtain the hydrochloride.

Synthesis of [^{15}N]Hydroxyethylhydrazine Hydrochloride. To a solution of 1.14 mmol of NaOH in absolute ethanol was added [$^{15}N_2$]hydrazine sulfate (0.48 mmol), and the suspension was stirred for 24 h. Bromoethanol (0.48 mmol) was added and allowed to react overnight at room temperature. The reaction mixture was diluted to 0.50 L with water and chromatographed on Dowex 50 × 8 (H^+ form). The resin was washed with water, and the hydrazine was eluted with 1 N HCl. Fractions were spotted onto silica gel TLC plates and HEH-containing fractions were identified using conjugation with (*N*,*N*-dimethylamino)benzaldehyde. Peak fractions were combined and dried by rotary evaporation. The residue was dissolved in water and subjected to rotary evaporation to remove trace HCl. ^{1}H NMR spectrum of the product confirmed the identity of the material.

EPR Spectroscopy of Samples in H_2O and in ^2H_2O. EAL (~26 mg mL^{-1} in 10 mM Hepes/NaOH, pH 7.5) was exchanged into ^2H_2O by lyophilization and resuspension in ^2H_2O. Control samples of EAL were also lyophilized but redissolved in H_2O. Separate stock solutions of HEH and coenzyme B_{12} were prepared in ^2H_2O and H_2O. The samples contained HEH (10 mM), coenzyme B_{12} (0.6 mM), Hepes/NaOH, pH 7.5 (16 mM), and EAL (21 mg mL^{-1}). The mixtures were transferred to EPR tubes and frozen within 20−30 s of mixing the ingredients.

EPR Measurements. EPR spectra were recorded at X-band on a Varian E-3 spectrometer. A standard liquid nitrogen immersion Dewar was employed to maintain samples at 77 K. Spectra obtained with the unlabeled HEH and [$^{15}N_2$]HEH in ^2H_2O were resolution enhanced as previously described (*23*). A Hanning window function was used in apodization.

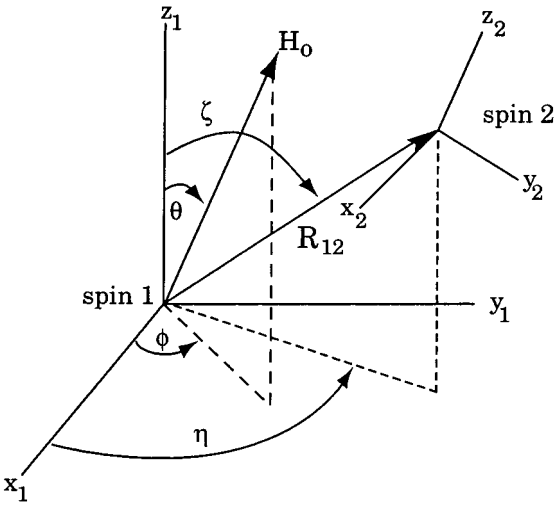

FIGURE 1: Schematic representation of the coordinate system describing the orientation of a second spin (spin 2) and of the magnetic field H_o, with respect to the principal axis of spin 1. The orientation of the magnetic field is specified by the angles θ and ϕ. The orientation of the interspin vector, R_{12}, is specified by the spherical angles ζ and η. Eulerian angles (α,β,γ) specify the orientation of the principal axis of spin 2 with respect to that of spin 1.

Analysis of the EPR Spectra. The active sites of EAL are expected to generate two paramagnetic species—a substrate-derived radical and the low-spin Co^{2+} of B_{12r}—in relatively close proximity. An exchange interaction and a through-space, dipole−dipole interaction are expected to arise from the proximity of the two paramagnetic centers. The framework for treatment of the combined effects of exchange and dipole−dipole coupling of unpaired electron spins has been presented previously (*24*−*26*). In the analysis of the EPR spectra, terms that need to be considered include the Zeeman interaction of each electron spin with the laboratory magnetic field, the exchange and dipole−dipole interactions between the electron spins, and the nuclear hyperfine interactions at each center. The spectra are interpreted with the following spin Hamiltonian:

$$H_S = \beta\vec{H}\cdot\mathbf{g_1}\cdot\vec{S}_1 + \beta\vec{H}\cdot\mathbf{g_2}\cdot\vec{S}_2 + J_o\vec{S}_1\cdot\vec{S}_2 + \vec{S}_1\cdot\mathbf{D}\cdot\vec{S}_2 + H_{HF} \quad (1)$$

where $\vec{H}$ is the laboratory magnetic field, $\mathbf{g_1}$ and $\mathbf{g_2}$ are the g tensors of the low-spin Co^{2+} and radical, respectively, J_o is isotropic exchange coupling constant, $\mathbf{D}$ is the dipole−dipole tensor, and H_{HF} represents the first-order hyperfine terms for each center:

$$H_{HF} = \sum_{j=1}^{n} K_j(\theta,\phi)\hat{I}_{jz}\hat{S}_{1z} + \sum_{k=1}^{m} K_k(\theta,\phi)\hat{I}_{kz}\hat{S}_{2z} \quad (2)$$

where $K(\theta,\phi)$ is the hyperfine interaction for a particular nucleus along the magnetic field direction (*27*). The smaller nuclear Zeeman and nuclear quadrupole interaction terms were neglected in the analysis. The various interaction terms are diagonal in their individual principal axis systems, and orthogonal transformations are required to bring all of the interactions into a common frame of reference. These rotations become part of the parameter space that needs to be explored in simulations. The general coordinate system is shown in Figure 1.

A complicating factor in the present case of a low-spin Co^{2+} is the *g* anisotropy at this center. The spectrum for B_{12r} bound to EAL exhibits axial symmetry ($g_\perp = 2.26$; $g_\parallel = 2.01$). Because of the *g* anisotropy of Co^{2+}, the dipole−dipole interaction is no longer represented by a traceless, symmetric tensor, and the exchange interaction is no longer a scalar quantity. Rather, the dipole−dipole and exchange interactions each consists of a scalar, a vector, and a traceless, symmetric tensor (*28*). The scalar part of the dipole−dipole interaction gives an isotropic splitting that will add to the isotropic exchange interaction. The *g* anisotropy of Co^{2+} gives rise to a rhombic (E) term in the zfs tensor describing the dipole−dipole interaction whenever the interspin vector is not aligned with a principal axis of low-spin Co^{2+} (*29*). The *g* anisotropy of the low-spin Co^{2+}, can also lead to anisotropies in the exchange interaction (*25*). The anisotropic components of the exchange and dipole−dipole interactions are combined into the term, $\vec{S}\cdot\mathbf{D}\cdot\vec{S}$, where **D** is a conventional zfs tensor. This zfs interaction, expressed in a spherical basis and rotated into the laboratory axis system, becomes (*30*)

$$H_{zfs} = D_o[3S_z^2 - S(S+1)] + D_{+1}(S_+S_z + S_zS_+) + D_{-1}(S_zS_- + S_-S_z) + D_{+2}(S_+^2) + D_{-2}(S_-^2) \quad (3)$$

The coefficients D_o, D_{+1}, D_{-1}, D_{+2}, and D_{-2} are

$$D_o = \frac{D}{6}(3\cos^2\theta - 1) + \frac{E}{2}\sin^2\theta\cos 2\phi \quad (4)$$

$$D_{\pm 1} = \left(\frac{1}{4}\sin 2\theta\right)(-D + E\cos 2\phi) \pm \frac{i}{2}E\sin\theta\sin 2\phi \quad (5)$$

$$D_{\pm 2} = \frac{1}{4}[D\sin^2\theta + E\cos 2\phi\,(1+\cos^2\theta)] \pm \frac{i}{2}E\cos\theta\sin 2\phi \quad (6)$$

Computational Strategies. Powder pattern spectra were obtained by numerical integration of the following expression (*27*):

$$\frac{dF}{dH} = \int_0^{2\pi}\int_0^{\pi}\frac{dG}{dH}\sin\theta\,d\theta\,d\phi \quad (7)$$

where θ and ϕ are the polar and azimuthal angles that relate the applied magnetic field direction (H_o) to the molecular frame (Figure 1).

Some simplifications accrue from the properties of the two paramagnetic centers. For example, because of the axially symmetric *g*-tensor of the low-spin Co^{2+}, the spherical angle η (Figure 1) is not needed to specify the magnitude of the spin of Co^{2+}.

The energy matrix, which was block diagonal, was set up as described previously (*28*) (see Table 1). The following procedure was used to generate a magnetic field-swept spectrum. For a given combination of angles, θ and ϕ, the matrix was diagonalized using the CH route of EISPACK (*31*) at field values above and below the range of interest. Energy level differences of allowed transitions were determined at both field values. A transition was presumed to occur in the range of interest if $\Delta E/h\nu$ was below unity at the lower field value and greater than unity at the upper value. To determine the position of the transition within the region of the spectrum, the two ΔE values were extrapolated to zero field, and the slope of the line was used to calculate where, within the field range, the transition would occur. This process yielded two position estimates for the transition. A more precise value of the field position was obtained by iterative recalculation of the energy matrix starting with the initial estimates of the field and continuing until the estimates obtained from the solving the energy levels at the upper and lower field limits agreed to <0.1 G. The speed of convergence is dependent on the magnitude of the off-diagonal elements, but transitions could typically be found in less than five iterations. The transition probabilities were evaluated from the matrix of the eigenvectors, and a Gaussian line shape was fitted at the transition. In each simulation, 2500 combinations of θ and ϕ were sampled in accordance with the solid angle integration of eq 7.

Table 1: Sample Block from the Energy Matrix

	$\lvert\alpha\alpha; I_mI_n\rangle$	$\lvert\alpha\beta; I_mI_n\rangle$	$\lvert\beta\alpha; I_mI_n\rangle$	$\lvert\beta\beta; I_mI_n\rangle$
$\langle\alpha\alpha; I_mI_n\rvert$	$\frac{1}{2}\beta hH(g_1+g_2) + \frac{1}{4}hJ + hD_o + \frac{1}{2}h(A_mI_m + A_nI_n)$	$\sqrt{2}\,hD_{+1}$	$\sqrt{2}\,hD_{+1}$	$2\,hD_{+2}$
$\langle\alpha\beta; I_mI_n\rvert$	$\sqrt{2}\,hD_{-1}$	$\frac{1}{2}\beta H(g_1-g_2) - \frac{1}{4}hJ - 2\,hD_o + \frac{1}{2}h(A_mI_m - A_nI_n)$	$\frac{1}{2}hJ$	$-\sqrt{2}\,hD_{+1}$
$\langle\beta\alpha; I_mI_n\rvert$	$\sqrt{2}\,hD_{-1}$	$\frac{1}{2}hJ$	$\frac{1}{2}\beta hH(-g_1+g_2) - \frac{1}{4}hJ - 2\,hD_o + \frac{1}{2}(-A_mI_m + A_nI_n)$	$-\sqrt{2}\,hD_{+1}$
$\langle\beta\beta; I_mI_n\rvert$	$2\,hD_{-2}$	$-\sqrt{2}\,hD_{-1}$	$-\sqrt{2}\,hD_{-1}$	$\frac{1}{2}\beta hH(-g_1-g_2) + \frac{1}{4}hJ + hD_o + \frac{1}{2}h(-A_mI_m - A_nI_n)$

Optimal fits to experimental spectra were obtained by systematically varying the parameters and visual inspection of the match between experimental and simulated patterns. Error limits were estimated by varying the parameters to achieve a noticeable degradation of the fit.

RESULTS AND DISCUSSION

Inactivation Kinetics. Incubation of EAL with coenzyme B_{12} and HEH leads to a rapid and complete loss of enzymatic activity. EAL was preincubated with 10 mM HEH and 0.34 mM coenzyme B_{12}, aliquots were withdrawn, diluted 100-fold, and assayed in the presence of saturating ethanolamine (10 mM) and cofactor (16 μM). Within 20 s of exposure to HEH, activity of EAL is reduced to 8% of control samples and is <1% after 15 min. No inactivation was observed if coenzyme B_{12} was omitted from the incubation mixtures.

Table 2: Quantitation of Inactivation Products

product	product/EAL[a]
B_{12r}/hydrazine cation radical[b]	6.0 ± 0.1
5′-deoxyadenosine	5.2 ± 0.4
acetaldehyde[c]	5.6 ± 0.1

[a] EAL concentration was based on the M_r of an $\alpha_6\beta_6$ complex (491 kDa). [b] The electron spin-spin coupling between the low−spin Co^{2+} of B_{12r} and the hydrazine cation radical establishes 1:1 stoichiometry of these two radicals. [c] Detected as the 2,4−dinitrophenylhydrazine derivative as described in the Experimental Procedures.

Fate of B_{12} during Inactivation of EAL by HEH. During the course of inactivation of EAL in the presence of excess coenzyme B_{12} and HEH, the cobalt−carbon bond of the coenzyme B_{12} is homolyzed to produce B_{12r}. The characteristic optical absorption features of B_{12r} are fully developed in the spectrum of the reaction mixture after ∼20 s, and no further changes are observed in the profile upon longer incubation (15 min, data not shown). In this experiment, an excess of coenzyme B_{12} (20-fold) was used to ensure occupancy of all active sites of the enzyme by cofactor. Using the difference extinction coefficient of coenzyme B_{12} versus B_{12r} one can estimate that ∼6 equiv of B_{12} is converted to B_{12r} during the inactivation (Table 2). The B_{12r} is tightly bound to the enzyme, and coenzyme B_{12} never reforms. Absorption spectra obtained after extensive dialysis of the enzyme show the 472 nm feature, which is characteristic of B_{12r} (data not shown).

Formation of B_{12r} during the course of the inactivation indicates that the carbon−cobalt bond of the cofactor is cleaved homolytically. Homolysis of this bond is also believed to occur as part of the normal catalytic cycle to produce the 5′-deoxyadenosyl radical and B_{12r}. The 5′-deoxyadenosyl radical then initiates catalysis by abstracting a hydrogen atom from the substrate to form 5′-deoxyadenosine and a substrate radical (*3*). To determine whether inactivation by HEH produces 5′-deoxyadenosine, EAL was incubated with coenzyme B_{12} and HEH for 15 min, and the reaction mixtures were quenched with acid, neutralized, and assayed by HPLC. These experiments show that ∼6 equiv of 5′-deoxyadenosine is produced during the inactivation (Table 2). Formation of 5′-deoxyadenosine requires that all components of the reaction, i.e., enzyme, coenzyme B_{12}, and HEH, be present.

Fate of HEH during Inactivation. The products of HEH during the inactivation were investigated, and acetaldehyde was identified as a product. The aldehyde was detected by derivatization with 2,4-dinitrophenylhydrazine, and the hydrazone was identified and quantitated by HPLC. Nearly 6 equiv of acetaldehyde was produced during the inactivation (Table 2). Formation of acetaldehyde required that all components of the assay, enzyme, coenzyme B_{12}, and HEH be present. Formation of acetaldehyde was essentially complete within the first 20 s.

Partial Recovery of EAL Following Inactivation by HEH. B_{12r} can be removed from EAL by precipitation of the protein with ammonium sulfate in acidic solution followed by resuspension of the protein in fresh buffer and dialysis (*7*). In the present case, this procedure restores ∼50% of the original enzymatic activity. The mechanism of the removal of B_{12r} from the protein is not completely understood; however, during the course of precipitation and dissolution of the protein, air oxidation of B_{12r} to hydroxo-B_{12} may occur. This oxidation may facilitate removal of the cofactor fragment. Indeed, the absorption spectrum of the supernatant from the acid ammonium sulfate precipitation is similar to that of hydroxo-B_{12}. In the subsequent dialysis step, hydroxo-B_{12} is removed leading to partial gain of activity. After this treatment, no form of B_{12} could be detected in the enzyme, as judged by the optical absorption spectrum (data not shown).

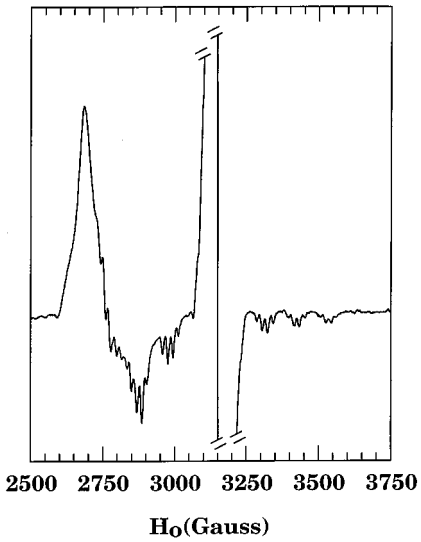

FIGURE 2: X-Band EPR spectrum of HEH-inactivated EAL showing presence of features corresponding to B_{12r} and a companion radical species with absorption near $g = 2.0$. The amplitude of the signal of the radical centered at $g = 2.0$ is off scale. The spectrometer frequency was 9.09 GHz and the spectrum was acquired at 4 mW microwave power.

EPR Spectra of the Inactivation Mixture. EAL was mixed with coenzyme B_{12} and with HEH, frozen after 20 s incubation, and examined by EPR. The EPR spectrum (Figure 2) confirms the presence of B_{12r} and reveals a strong signal of a radical centered near $g \approx 2$.

The g and A tensors of the low-spin Co^{2+} in B_{12r} are axially symmetric, and "turning points" in first-derivative spectra are observed with the magnetic field perpendicular and parallel to the half occupied d_{z^2} orbital of Co^{2+} (*32*). The hyperfine interaction from the ^{59}Co nuclear spin ($I = 7/2$) splits the EPR signals from the cobalt into an octet pattern. The ^{59}Co hyperfine splitting is typically unresolved ([^{59}Co] $A_\perp \sim 5-10$ G) for the magnetic field perpendicular to the d_{z^2} orbital. In the parallel direction, the hyperfine splitting from ^{59}Co is large ([^{59}Co] $A_{||} \approx 110$ G), and an octet pattern centered about $g_{||}$ is observed. A superhyperfine interaction between the unpaired electron of Co^{2+} and a ^{14}N ($I = 1$) of the lower axial ligand further splits the parallel features of B_{12r} into 1:1:1 triplets ([^{14}N] $A_{||} \approx 18$ G). However, in the EPR spectrum of EAL inactivated by HEH (Figure 2), the superhyperfine features of the ^{59}Co in the parallel direction are quartets with apparent intensities of 1:2:2:1. The possibility that the axial ^{14}N ligand had been displaced during the inactivation was initially considered. The multiplicities and intensities of the pattern were, however, inconsistent with the nuclear spin of potential new axial ligands. Rather, the quartet splitting pattern results from magnetic interactions between the unpaired spin of the B_{12r} and the radical in the active site. The total electron spin−spin interaction, $|J +$

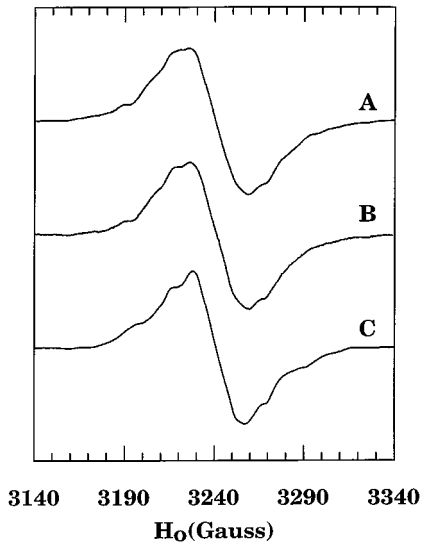

FIGURE 3: X-Band EPR spectra of EAL obtained after inactivation with unlabeled HEH (A), [1,1,2,2-$^2H_4$]HEH (B), and ^{15}N-labeled HEH (C). The microwave frequency was 9.09 GHz and the spectra were acquired at 0.5 mW microwave power.

$2D|$, along the $g_{||}$ direction of the Co axis system, coincidentally, matches the ^{14}N superhyperfine splitting such that $|J + 2D|$ adds a doublet splitting. The resulting splitting pattern is therefore that of an overlapping doublet of triplets, i.e., the 1:2:2:1 quartet pattern.

EPR Spectra with Isotopically Labeled HEH. The spectrum obtained with [1,1,2,2-$^2H_4$]HEH is identical to that obtained from unlabeled HEH (Figure 3). By contrast, in the spectrum obtained with [^{15}N]HEH, the hyperfine splitting manifold is altered relative to that of unlabeled HEH. These observations indicate that the unpaired electron resides in the hydrazine fragment of HEH.

Coupling of the Radical to Solvent Exchangeable Protons. EPR spectra of EAL inactivated by HEH were obtained with samples prepared in H_2O and in ^2H_2O. EPR spectra of the radical regions of these samples are shown in Figure 4. Hyperfine structure within the envelope of the spectrum is considerably narrowed in the spectrum of the sample prepared in ^2H_2O. Narrowing of the signals in ^2H_2O is consistent with the presence of solvent exchangeable protons (deuterons) near to the center of unpaired spin. The hyperfine interaction from these protons contributes an inhomogeneous broadening to the EPR signals that is reduced upon substitution of ^{2}H ($\gamma^2_H/\gamma^1_H \approx 1/6.5$).

EPR spectra were further analyzed by simulation. Unlike the $g_{||}$ region of the spectrum of B_{12r}, which represents a unique (single-crystal like) direction, the spectrum of the radical is a "full-fledged" powder pattern wherein absorptions from all orientations of the center in the magnetic field are represented within the spectral envelope. The overall pattern is expected to have the line shape of a classical Pake doublet (*33*); however, splitting of the perpendicular peaks is modified to reflect $|J - D|$ whereas the parallel splitting is $|J + 2D|$. Modeling of this spectrum requires inclusion of all of the electron spin-spin interaction terms in the Hamiltonian as well as the anisotropic nitrogen hyperfine interaction, and *g* anisotropy of the hydrazine fragment. Simulations of the EPR spectra obtained with the unlabeled and with [$^{15}N_2$]HEH are shown in panels A and B of Figure 5,

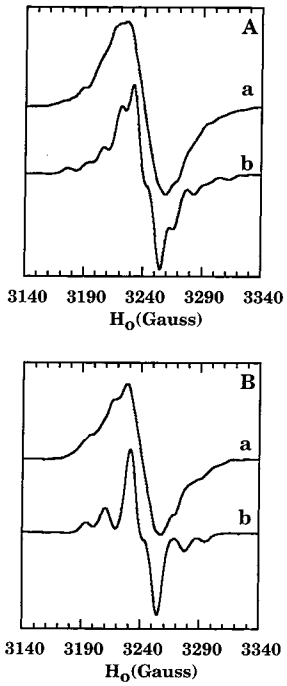

FIGURE 4: Comparison of EPR spectra obtained by inactivating EAL with unlabeled HEH (A) or ^{15}N-labeled HEH (B) in H_2O (Aa,Ba) or ^2H_2O (Ab,Bb). The microwave frequency was 9.09 GHz and the spectra were acquired at 0.5 mW microwave power.

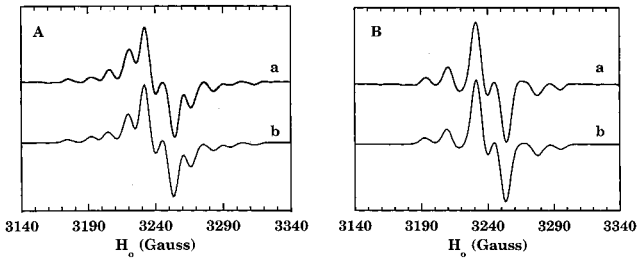

FIGURE 5: Comparison of resolution enhanced experimental and simulated EPR spectra obtained with unlabeled or ^{15}N-labeled HEH. The experimental EPR spectra are of samples prepared in ^2H_2O with either unlabeled (Aa) or ^{15}N-labeled (Ba) HEH. The simulations of the spectra from unlabeled (Ab) HEH and from ^{15}N-labeled (Bb) HEH were performed using a line width of 4.5 G and other parameters as listed in Table 3.

respectively. The parameters used for the simulations are listed in Table 3. The analysis indicates that the odd electron is shared equally by both nitrogens of the hydrazine moiety—a result that is consistent with results from single—crystal EPR studies of the hydrazine cation radical (*34*). Moreover, the isotropic component of the nitrogen hyperfine interaction is, as expected, about half of that reported for the ammonia radical cation (*35*). Best fits are obtained with the *g* and *A* tensors of the radical rotated 90° with respect to the *z* axis of the coordinate system of the low-spin Co^{2+} (Figure 6).

The absolute signs of *J* and *D* are indeterminate from the spectra. The spectra do, however, reflect the relative signs of these two magnetic interaction terms, and successful simulation requires that $|D| > |J|$ and that the two parameters have opposite signs. The magnetic interaction terms which reproduce the patterns in the radical also model the quartet splittings in the $g_{||}$ features of B_{12r} (see Figure 7). This observation, together with the absence of a requirement for a rhombic term in the zfs interaction, suggests that the radical

Table 3: Parameters Used to Simulate EPR Spectra of the Hydrazine Cation Radical[a]

		Euler angles (deg)[b]		
parameters	principal values	α	*β*	*γ*
g (B_{12r})[c]	2.26			
	2.26			
	2.01			
g (radical)[d]	2.0043			
	2.0037	0	90	*e*
	2.0021			
J[f]	$+5.5 \pm 1.0$ G			
D	-12.5 ± 1.0 G			
E	0 G			
$^{14}N_{1,2}$	2.5 G			
	2.5 G	0	90	*e*
	30 G			
$^{15}N_{1,2}$	3.5 G			
	3.5 G	0	90	*e*
	42 G			

[a] Simulations were carried out as described in the Experimental Procedures. To reduce the computational times, the cobalt nuclear spin ($I = 7/2$) was not included in the calculations. In the simulations of the radical region, the contributions to the simulation from the low−spin Co^{2+} were suppressed from the output of the program. [b] The Euler angles were defined as described by Rieger *(47)*. [c] The *g*-frame of the Co^{2+} was chosen as the reference frame for the rotations. [d] The *g*-tensor is within experimental error of that reported for the hydrazine cation radical (*34*). [e] The simulations are insensitive to the *γ* angle. [f] The value of *J* obtained from the simulations contains a contribution from the isotropic component of the dipolar interaction of $J_d = (-2\beta^2/3R^3)g_2\Delta g_1 \approx -1.2$ G, where g_2 is the isotropic *g*-value of the radical and Δg_1 is $(g_\perp - g_{||})$ of Co^{2+} (*28*).

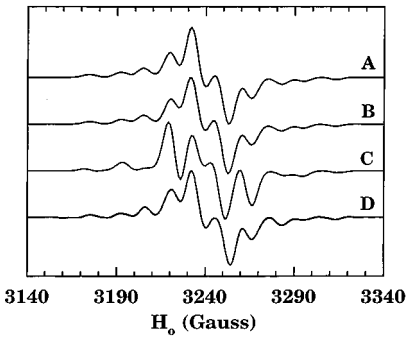

FIGURE 6: Comparison of simulated spectra obtained by orienting the *g*- and A-tensors of the hydrazine cation radical along the (A) *x*, (B) *y*, or (C) *z* direction of the principal axis system of low-spin Co^{2+} (see Figure 1), and (D) is the EPR spectrum obtained when EAL is inactivated with unlabeled HEH in D_2O. The parameters used in the simulations are listed in Table 3.

lies close the *z*-axis of the low-spin Co^{2+} in B_{12r}. However, the *g* anisotropy of the low-spin Co^{2+} is too small to make the dipole−dipole interaction very sensitive to the position of the interspin vector in the *g*-frame of Co^{2+} (*36*).

These EPR results identify the radical as the hydrazine cation radical. The ultimate fate of this species has not been explored, although the radical persists for at least 20 min at room temperature. Presumably, the radical would eventually be quenched either before or after escaping the confines of the active site. The electron spin−spin coupling reflected in the EPR spectra shows that there is a 1:1 stoichiometry of B_{12r} and the hydrazine cation radical.

The distance dependence of the spin−spin interactions may be exploited to estimate the separation between the hydrazine cation radical and Co^{2+} of B_{12r}. Buettner and Coffman (*37*)

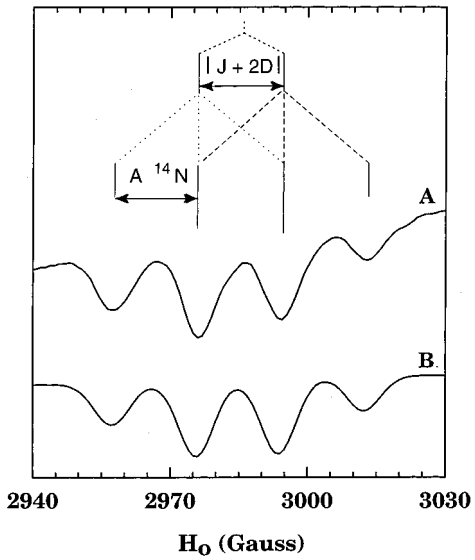

FIGURE 7: Comparison of experimental (A) and simulated (B) EPR spectra of one of the ^{59}Co parallel hyperfine features. The parameters used in the simulation are listed in Table 3.

have provided an empirical limit function which relates *J* (cm^{-1}) to the distance, *R*(Å):

$$|J| \leq 1.35 \times 10^7 \, e^{-1.8R} \quad (8)$$

This expression and the value of *J* determined from the analysis of the spectra led to a distance estimate of $R \leq 13$ Å between B_{12r} and the radical.

The dependence of the dipole−dipole parameter *D* (G) on the distance *R* (Å) between the two paramagnetic centers using the point dipole approximation (*38*) is

$$D = 6.95 \times 10^3 \, g_1 g_2 / R^3 \quad (9)$$

Using this equation, one can estimate that the hydrazine cation radical and B_{12r} are separated by 13 Å. Use of eq 9 implies a point dipole approximation and the absence of anisotropic exchange or antisymmetric exchange contributions. The agreement between the distance estimates from the separate magnetic interaction terms is reassuring. A schematic representation of the results from the analysis of the EPR data is shown in Scheme 1.

Stoichiometry of Products to Active Sites. The inactivation of EAL by HEH converts coenzyme B_{12} into B_{12r} and 5′-deoxyadenosine, and HEH is converted to acetaldehyde and a hydrazine cation radical (eq 10):

$$\text{HEH} + \text{coenzyme } B_{12} \xrightarrow{\text{EAL}} \left\{ \begin{array}{l} 5'\text{-deoxyadenosine} \\ B_{12r} \\ \text{acetaldehyde} \\ \text{hydrazine cation radical} \end{array} \right\} \quad (10)$$

Results from equilibrium titrations of EAL with analogues of coenzyme B_{12} suggested that there were two active sites per $\alpha_6\beta_6$ oligomer (*13, 14, 39*). However, experiments based on the steady-state level of B_{12r} during turnover suggested that six active sites were present (*16*). The inactivation of EAL with HEH in the presence of coenzyme B_{12} produces ~6 equiv of 5′-deoxyadenosine, B_{12r}, the hydrazine cation

Scheme 1

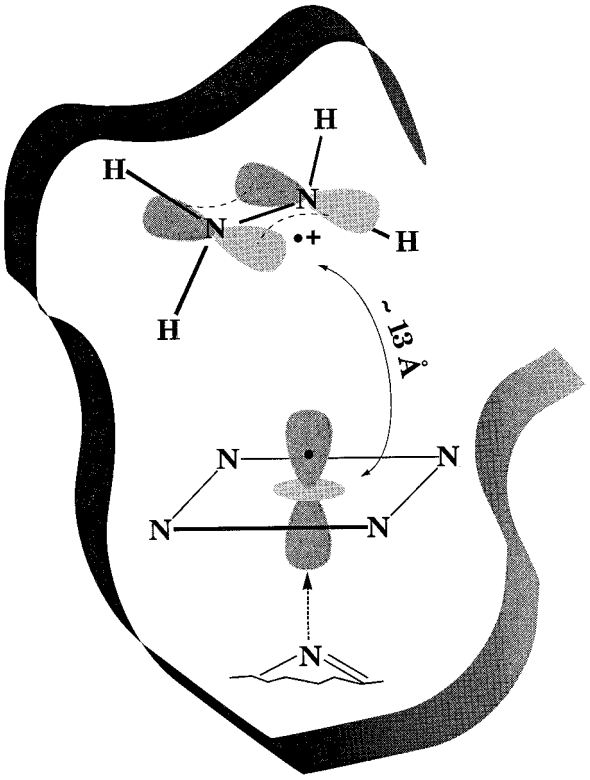

radical, and acetaldehyde. B_{12r} is not easily removed from the enzyme, and it is unlikely that B_{12r} is exchanged for fresh coenzyme B_{12}. Thus, the HEH inactivation indicates that six active sites are present in the $\alpha_6\beta_6$ oligomer of EAL.

Mechanism of Inactivation. A plausible mechanism for the inactivation that is consistent with all of the experiments is shown in Scheme 2. The similarity of HEH to ethanolamine allows binding of the analogue. This binding sets the stage for the reaction, i.e., formation of an HEH radical and B_{12r}. Substituted alkyl free radicals can fragment in either polar or homolytic processes (*40*). For example, a propensity for homolytic cleavage has been noted for radicals of N-substituted ethanolamines (*41*). In the HEH radical, the relative stability of the hydrazine cation radical (*35*) undoubtedly tips the balance toward homolytic fragmentation, and the homolytic option diverts the intermediate from a catalytic cycle that could allow multiple turnovers. The presence of equimolar quantities of acetaldehyde and 5′-deoxyadenosine rules out multiple turnovers of HEH. Studies with [1,1,2,2-$^2H_4$]HEH, however, indicate that the first step is reversible (*42*). The HEH radical can eliminate the hydrazine cation radical leaving the enol of acetaldehyde (Scheme 2, path A) or rearrange to a product radical before fragmentation (Scheme 2, path B). These two routes would lead to identical products, and the present experiments do not rule out either pathway. The inability (*43*) of the hydrazine cation radical to recapture a hydrogen atom from 5′-deoxyadenosine interrupts the cycle and leaves the enzyme stranded as an inactive complex having B_{12r} blocking the cofactor site.

The present results highlight the steep distance dependence of the spin−spin exchange term. In some coenzyme B_{12} dependent enzymes, intermediates are observed in which the two paramagnetic centers are close (6−7 Å) such that the exchange interaction ($|J| \approx 40$ cm^{-1}) dominates the EPR spectra (*25, 26, 44*). In these situations, the EPR spectra correspond to those of a strongly coupled triplet spin system (*25, 26, 44*). For other systems, in which the separation of the radical from B_{12r} is only a few angstroms greater, the exchange and dipole−dipole interactions are of the same order of magnitude (*24, 45, 46*). The weakly coupled situation, wherein the two paramagnetic centers retain separate "EPR identities", is somewhat easier to deal with analytically. As illustrated in the present case, the EPR signals of the low-spin Co^{2+} and those of the radical provide complementary information that can serve as a internal validation of the parameters.

ACKNOWLEDGMENT

We are grateful to Ms. La Rosa Faust and Dr. Bernard Babior for providing the plasmid pKQE4.5.

Scheme 2

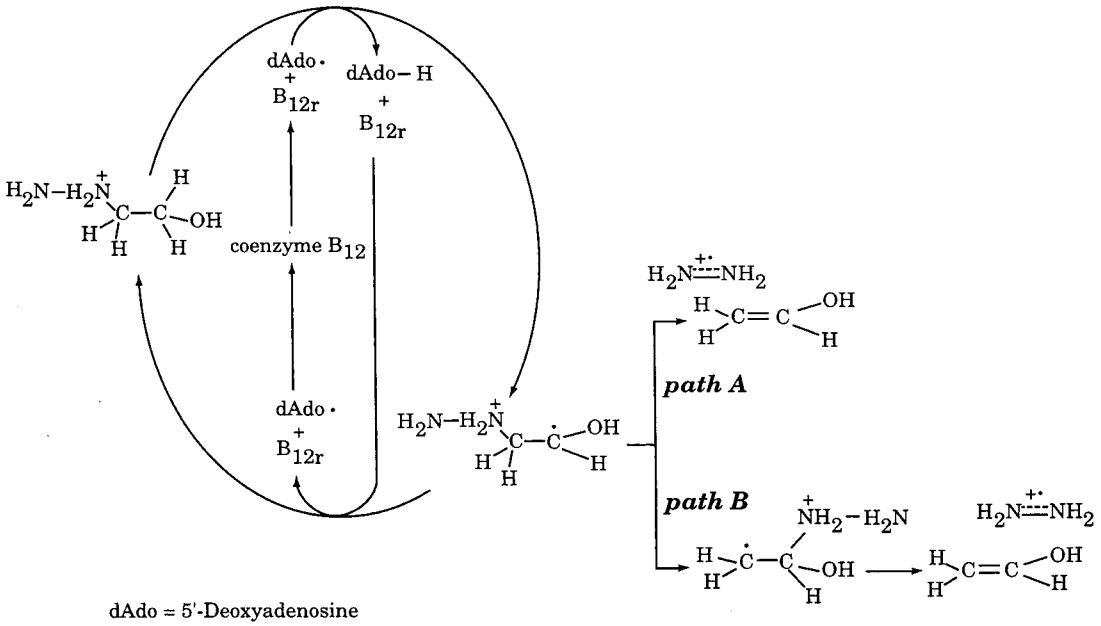

dAdo = 5′-Deoxyadenosine

REFERENCES

1. Bradbeer, C. (1965) *J. Biol. Chem. 240*, 4675−4681.
2. Babior, B. M. (1982) in *B_{12}* (Dolphin, D., Ed.) John Wiley & Sons, Inc., New York.
3. Babior, B. M. (1988) *BioFactors 1*, 21−26.
4. Blackwell, C. M., Scarlett, F. A., and Turner, J. M. (1976) *Biochem. Soc. Trans. 4*, 495−497.
5. Babior, B. M. (1970) *J. Biol. Chem. 245*, 1755−1766.
6. Graves, S. W., and Babior, B. M. (1982) *J. Biol. Chem. 257*, 4102−4105.
7. Kaplan, B. H., and Stadtman, E. R. (1968) *J. Biol. Chem. 243*, 1794−1803.
8. Stubbe, J., and van der Donk, W. (1998) *Chem. Rev. 98*, 705−762.
9. Wagner, O. W., Lee, H. A., Jr., Frey, P. A., and Abeles, R. H. (1966) *J. Biol. Chem. 241*, 1751−1762.
10. Stubbe, J. (1990) *Adv. Enzymol. Relat. Areas Mol. Biol. 63*, 349−417.
11. Silva, D. J., Stubbe, J., Samano, V., and Robins, M. J. (1998) *Biochemistry 37*, 5528−5535.
12. van der Donk, W. A., Yu, G., Perez, L., Sanchez, R. J., Stubbe, J., Samano, V., and Robins, M. J. (1998) *Biochemistry 37*, 6419−6426.
13. Babior, B. M. (1969) *J. Biol. Chem. 244*, 2927−2934.
14. Babior, B. M., and Li, T. K. (1969) *Biochemistry 8*, 154−160.
15. Faust, L. P., and Babior, B. M. (1992) *Arch. Biochem. Biophys. 294*, 50−54.
16. Hollaway, M. R., Johnson, A. W., Lappert, M. F., and Wallis, O. C. (1980) *Eur. J. Biochem. 111*, 177−188.
17. Faust, L. P., Connor, J. A., Roof, D. M., Hoch, J. A., and Babior, B. M. (1990) *J. Biol. Chem. 265*, 12462−12466.
18. Swanson, B. A., and Frey, P. A. (1993) *Biochemistry 32*, 13231−13236.
19. Kaplan, B. H., and Stadtman, E. R. (1971) *Methods Enzymol. 17*, 818−824.
20. Hollaway, M. R., White, H. A., Joblin, K. N., Johnson, A. W., Lappert, M. F., and Wallis, O. C. (1978) *Eur. J. Biochem. 82*, 143−154.
21. Marsh, E. N. G., and Ballou, D. P. (1998) *Biochemistry 37*, 11864−11872.
22. Frey, P. A., Essenberg, M. K., and Abeles, R. H. (1967) *J. Biol. Chem. 242*, 5369−5377.
23. Latwesen, D. G., Poe, M., Leigh, J. S., and Reed, G. H. (1992) *Biochemistry 31*, 4946−4950.
24. Buettner, G. R., and Coffman, R. E. (1977) *Biochim. Biophys. Acta 480*, 495−505.
25. Bothe, H., Darley, D. J., Albracht, S. P., Gerfen, G. J., Golding, B. T., and Buckel, W. (1998) *Biochemistry 37*, 4105−4113.
26. Gerfen, G. J., Licht, S., Willems, J. P., Hoffman, B. M., and Stubbe, J. (1996) *J. Am. Chem. Soc. 118*, 8192−8197.
27. Hecht, H. G. (1967) *Magnetic Resonance Spectroscopy*, John Wiley & Sons, Inc., New York.
28. Eaton, G. R., and Eaton, S. S. (1989) in *Spin Labeling: Theory and Applications* (Berliner, L. J., and Reuben, J., Eds.) 650 pp, Plenum Press, New York.
29. Boas, J. F. (1984) in *Copper Proteins and Copper Enzymes* (Lontie, R., Ed.) 223 pp, CRC Press, Inc., Boca Raton.
30. Reed, G. H., and Markham, G. D. (1984) *Biol. Magn. Reson. 6*, 73−142.
31. Smith, B. T., Boyle, J. M., Dongarra, J. J., Garbow, B. S., Ikebe, Y., Klema, V. C., and Moler, C. B. (1976) *Matrix Eigensystem Routines - Eispack Guide*, Springer-Verlag.
32. Pilbrow, J. R. (1982) in *B_{12}* (Dolphin, D., Ed.) pp 431−463, John Wiley & Sons, Inc., New York.
33. Pake, G. E. (1948) *J. Chem. Phys. 16*, 327−336.
34. Edlund, O., Lund, A., and Nilsson, Å. (1968) *J. Chem. Phys. 49*, 749−755.
35. Bauld, N. L. (1997) *Radicals, Ions Radicals, and Triplets*, p 145, Wiley-VCH, New York.
36. Bandarian, V. (1998) Ph.D. Dissertation, University of Wisconsin, Madison.
37. Coffman, R. E., and Buettner, G. R. (1979) *J. Phys. Chem. 83*, 2387−2392.
38. Luckhurst, G. R. (1976) in *Spin Labeling: Theory and Applications* (Berliner, L. J., Ed.) 592 pp, Academic Press, New York.
39. Babior, B. M. (1969) *J. Biol. Chem. 244*, 2917−2926.
40. Giese, B. (1986) *Radicals in Organic Synthesis: Formation of Carbon-Carbon Bonds*, Pergamon Press, New York.
41. Gilbert, B. C., Larkin, J. P., and Norman, R. O. C. (1972) *J. Chem. Soc., Perkin Trans 2*, 794−802.
42. Bandarian, V., Poyner, R. R., and Reed, G. H. (1999) *Biochemistry 38*, 12403−12407.
43. Nelson, S. F. (1973) in *Free Radicals* (Kochi, J. F., Ed.) pp 581−583, John Wiley & Sons, Inc., New York.
44. Padmakumar, R., and Banerjee, R. (1995) *J. Biol. Chem. 270*, 9295−9300.
45. Schepler, K. L., Dunham, W. R., Sands, R. H., Fee, J. A., and Abeles, R. H. (1975) *Biochim. Biophys. Acta 397*, 510−518.
46. Boas, J. F., Hicks, P. R., Pilbrow, J. R., and Smith, T. S. (1978) *J. Chem. Soc., Faraday II 74*, 417−430.
47. Rieger, P. H. (1982) *J. Magn. Reson. 50*, 485−489.

BI990620G